RESEARCH ARTICLE

Study on the dynamic modelling method of a coilable mast based on hinge equivalent rotational stiffness identification

Y. Liu[1], L. Sun[1], H. Huang[1], W. Li[1] and X. Zhao[2]

[1]School of Astronautics, Beihang University, Beijing, China
[2]Institute of Remote Sensing Satellite, China Academy of Space Technology, Beijing, China
Corresponding author: L. Sun; Email: sunliang@buaa.edu.cn

Abstract

With numerous applications of coilable masts in high-precision space application scenarios, there are also greater demands on the accuracy of their dynamic modelling and analysis. The modelling of hinges is a critical issue in the dynamic modelling of coilable masts, which significantly affects the accuracy of the dynamic response analysis. For coilable masts, the rotational effect is the most important problem in hinge modelling. However, few studies have focused on this topic. To address this problem, the concept of hinge equivalent rotational stiffness is proposed in this paper to describe the rotational effect of the coilable mast hinges. After that, a new coilable mast dynamic model containing the undetermined hinge equivalent rotational stiffness is introduced, and an identification method for the hinge equivalent rotational stiffness based on the hammer test is proposed. Finally, the dynamic modelling method is validated through an actual coilable mast example, and the analysis and test results show that the accuracy of the dynamic model established by the proposed method in this paper is greater than that of the traditional model.

Nomenclature

|	
K_{hinge}	Hinge equivalent rotational stiffness
F_l	Tension of diagonal cable
F_{lr}, F_{lt}	Radial and tangential components of diagonal cable tension
l	Elongation of diagonal cable
	Torsional angle of hinge
ini	Initial stress of diagonal cable
L_{ini}	Initial preload of diagonal cable
S_{diag}	Cross-sectional area of diagonal cable
act	Actual stress of diagonal cable
act	Actual strain of diagonal cable
TMURS	Two mass points-undetermined rotational stiffness
HTM	Hammer test method
VHTM	Virtual hammer test method
K	Hinge rotational stiffness
f_1, f_2	Analytical results for first and second order frequencies
f_{t1}, f_{t2}	Test results for first and second order frequencies
MISO	Multiexcitation input and single response output
SIMO	Single excitation input and multiresponse output
FFT	Fast fourier transform

1.0 Introduction

Deployable structures are a class of structures that can be stowed in a narrow envelope during the rocket launch phase and deployed after the spacecraft enters orbit. They have been widely applied in space missions such as space station construction, earth observation and deep space exploration [1–3]. Coilable masts are among the most commonly used types of deployable structures and are particularly useful for small satellite missions because of their high packing coefficient and high strength-to-weight ratio [4, 5]. To date, there are many examples of successful in-orbit applications of coilable masts, such as GOES Astromast [6], Akebono Satellite Simplex Mast [7], ST8 Sailmast [8, 9] and the ISP solar sail mast [10, 11]. Beihang University (BUAA) successfully developed a 2-metre-high coilable mast and completed in-orbit deployment verification in the APSCO SSS-1 satellite mission [12].

With the continuous development of coilable mast technology, coilable masts have also been used in optical applications. JAXA applied a coilable mast to the X-ray astronomical satellite Hitomi to provide a 12 m focal length for hard X-ray telescopes and imagers [13–15]. NASA applied a coilable mast in the Imaging X-ray Polarimetry Explorer (IXPE) to provide a 4 m focal length for the X-ray telescopes and detectors [16, 17]. Unlike ordinary deployment tasks, the above optical applications have higher precision requirements for coilable masts because they are directly related to the alignment accuracy of the optical path. In orbit, the vibration of a coilable mast caused by the attitude manoeuvres of the spacecraft and the atmospheric environment are the key factors that may cause misalignment of the optical path and failure of the entire mission. Therefore, a more accurate model of the coilable mast is necessary to predict the dynamic responses of the coilable mast more accurately, which is beneficial to the design and performance evaluation of the optical system containing the coilable mast.

The typical configuration and components of coilable masts are shown in Fig. 1 [18, 19]. It consists of three longerons and a series of battens, diagonal cables and hinges. The methods for modelling longerons, battens and diagonal cables are mature. The problem encountered in modelling hinges is a key issue that affects the accuracy of the coilable mast model. Therefore, it is necessary to develop modelling methods for coilable masts that consider the influence of hinges to predict their dynamic response more accurately. However, current studies on coilable masts have focused mainly on the structural stability and buckling load [20, 21] and the dynamic and static characteristics during deployment and retraction [22, 23]. Only a few studies are related to the modelling and dynamic analysis of a coilable mast in the deployed state. Han studied the dynamic modelling and fundamental frequency analysis method of a coilable mast considering slack in diagonal cables [24]. Fan studied and analysed the influence of the preload of diagonal cables on the fundamental frequency of a coilable mast [25]. These studies focused on the diagonal cables of coilable masts but did not consider the influence of hinges.

Dynamic modelling and analysis problems that consider the effects of hinges have received more attention in other types of deployable structures, especially articulated truss masts [26]. On the basis of existing studies, hinge models can be categorised into three types: permanent contact models, two-state models and three-state models [27]. The permanent contact model ignores hinge clearances and assumes that the hinges are always in contact during motion. The two-state model considers the effects of two states of hinge clearances, separation and contact, on the dynamic response of structures. The three-state model considers one more state of the hinge clearances, the collision state, than the two-state model does. The three-state model is currently more widely studied because it describes all possible states of hinge clearances. Dubowsky and Freudenstein proposed 'an impact pair' model based on Hertz theory to address the contact force and collision depth in hinge clearances [28, 29]. Bauchau and Rodriguez proposed a method to describe the kinematics of hinges by considering nonlinear factors such as clearance, friction and lubrication [30]. Zhang proposed a hinge equivalent model considering clearance, nonlinear stiffness, friction and collision damping, and established a dynamic model of an articulated truss mast [26].

However, these models are not suitable for modelling the hinges of coilable masts. Since the hinges of articulated truss masts are locked when the mast is fully deployed, the nonlinearity caused by hinge clearances becomes the main factor affecting the dynamic response. Unlike articulated truss masts, the
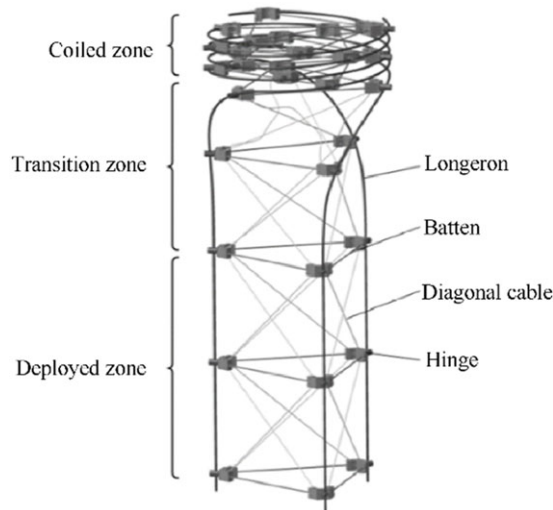
Figure 1. *Configuration and components of a coilable mast.*

hinge clearances of coilable masts can be almost eliminated under the preloading of diagonal cables, so the contact and collision nonlinearities caused by hinge clearances are not obvious. For coilable masts, the most important feature of their hinges is the rotational effect. This is because the coilable mast hinges are unlocked when fully deployed, and their rotational motion is limited to only four connected diagonal cables, as shown in Fig. 1. Under this weak constraint, the hinges of the coilable masts are more prone to rotation under external loads. Therefore, the rotation problem is the primary problem in the dynamic modelling of coilable mast hinges rather than the nonlinear contact and collision problems caused by hinge clearances.

In this paper, the concept of hinge equivalent rotational stiffness of coilable masts is proposed to describe the rotational effect of hinges, and a dynamic modelling method based on the identification of hinge equivalent rotational stiffness is proposed and experimentally verified. In Section 2.0, the coilable mast model considering hinge equivalent rotational stiffness is presented. In Section 3.0, the identification method for the hinge equivalent rotational stiffness is introduced. In Section 4.0, an actual coilable mast is used as an example for modelling and parameter identification, and the correctness of the model is verified experimentally.

2.0 Dynamic model of coilable masts containing hinge equivalent rotational stiffness

Coilable masts can be considered a special type of truss structure after deployment. However, unlike traditional truss structures with higher stiffness, coilable masts are more flexible and have hinges, diagonal cables and other components with nonlinear properties, which makes the modelling of coilable masts more complicated. The rotational effect of the hinge is the most important feature of coilable masts that distinguishes them from other truss structures. In this section, the concept of hinge equivalent rotational stiffness is presented first, and a new coilable mast dynamic model considering the hinge equivalent rotational stiffness is proposed.

2.1 Concept of hinge equivalent rotational stiffness

Hinges are important components of a coilable mast that are used to connect longerons, battens and diagonal cables. A typical hinge of a coilable mast is shown in Fig. 2, which consists of two parts that
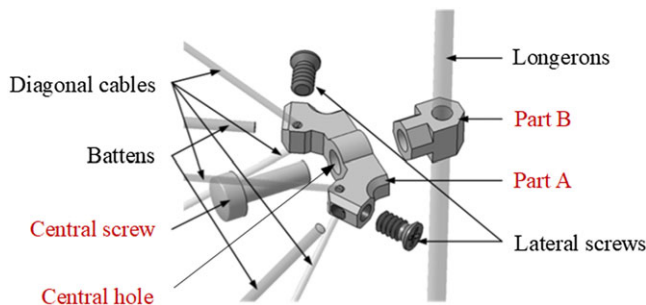
Figure 2. *Typical hinge of a coilable mast.*
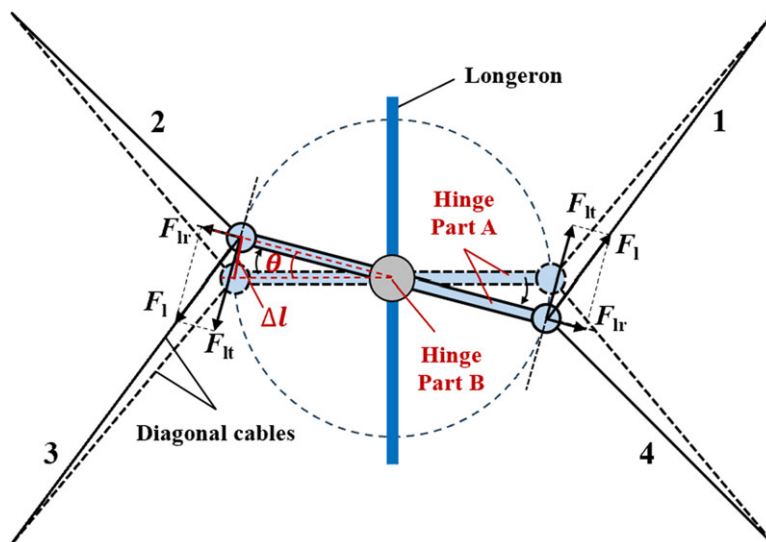
Figure 3. *Force analysis of hinge rotation.*

can rotate relative to each other, Part A and Part B. Part A is rigidly connected with the battens and diagonal cables, and Part B is rigidly connected with the longeron. The central screw and central hole form the rotating pair between Part A and Part B.

Unlike the locked hinges of articulated masts, the main feature of coilable masts is that their hinges can rotate slightly after deployment. Therefore, modelling the hinge rotational effect is a key factor affecting the overall modelling accuracy of coilable masts. The simulation results show that the frequency response obtained by ignoring the hinge rotational effect in modelling is inconsistent with the experimental results in terms of natural frequencies and modal shapes. In this study, the concept of the hinge equivalent rotational stiffness K_{hinge} is proposed to describe the rotational stiffness of the hinge. The higher its value is, the more difficult it is for the hinge to rotate, and conversely, the easier it is to rotate. K_{hinge} is positive infinity for locked hinges and zero for the case of free rotation.

The forces on the hinge during rotation are qualitatively analysed to facilitate understanding of the significance of the hinge equivalent rotational stiffness. In the case of small angle rotation, the diagonal cables play a major role in the hinge rotation process. As shown in Fig. 3, when the hinge and diagonal cables are in equilibrium, as shown by the dotted line, the tensions on the diagonal cables at positions 1–4 are equal. When the hinge rotates, the diagonal cables at positions 1 and 3 are pulled, and their tensions increase, whereas the tensions of the diagonal cables at positions 2 and 4 decrease or even slacken. Assuming that the tension at positions 1 and 3 at this time is F_1, the radial and tangential components of F_1 are F_{1r} and F_{1t}, respectively. F_{1t} will produce a restoring moment to return the hinge to its equilibrium
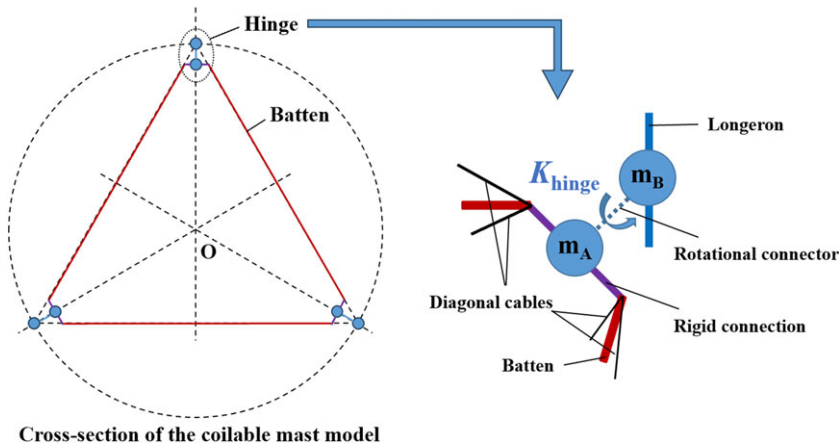
Figure 4. *TMURS model of the rotating hinge.*

position, and this restoring moment will increase as the hinge rotational angle increases. In the case of a small angle of rotation, the elongations of the diagonal cables Δl increase linearly with the torsional angle θ, as shown in Fig. 3, so the tensions of the diagonal cables and the restoring moment also increase linearly with the torsional angle; thus, at this time, K_{hinge} is a constant. In the case of a large angle of rotation, the longeron and battens connected to the hinge undergo nonnegligible deformation, making the force situation during the rotation of the hinge very complicated. At this time, the error of the linear assumption is large, and considering only K_{hinge} as a constant is not applicable to the modelling of this situation.

However, in practical engineering applications, the large angle of rotation of the hinge generally occurs only when the tip mass of the coilable mast is too large and the mast is highly flexible. In this case, the coilable mast may vibrate substantially or even buckle locally or completely under the effect of a large inertial force. Since this situation poses risks to the normal application of the coilable mast and the spacecraft platform with the mast, it is usually avoided at the design stage. Therefore, in most practical engineering applications, the hinge of the coilable mast does not experience a large angle of rotation, and the linear assumption made in this study, i.e., the case where K_{hinge} is constant, is applicable to most scenarios.

2.2 Model of the rotating hinge

On the basis of the concept of hinge equivalent rotational stiffness, a 'two mass points – undetermined rotational stiffness' (TMURS) hinge model is proposed, which is shown in Fig. 4. Unlike the traditional 'one mass point' hinge model, two mass points are used here to simulate the mass characteristics of the two parts of the hinge, Part A and Part B. A rotational connector is established between the two mass points, and the rotational connector is given a rotational stiffness K_{hinge} to describe the equivalent rotational stiffness of the hinge. The longerons, battens and diagonal cables are rigidly connected to the two mass points of the hinge.

K_{hinge} is an undetermined parameter that must be identified on the basis of experimental tests. The identification method for K_{hinge} is detailed in Section 3.0.

Remark: The nonlinearities of the hinge come mainly from the clearance, contact and collision of the hinge. They are ignored in the proposed hinge model in this paper. These nonlinearities are ignored because the clearance of the hinge is almost eliminated under the preloading of the diagonal cables, making the nonlinear characteristics of the hinge insignificant. Considering the nonlinearities introduced by hinge clearance, contact and collision on the basis of the proposed hinge model will further improve
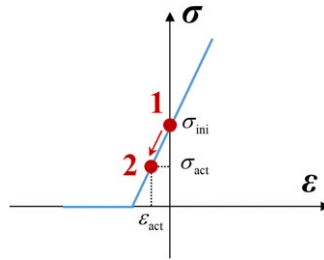
Figure 5. *Rebalancing process of coilable mast preloads.*

the accuracy of the overall model of the coilable mast. According to the literature, when considering the hinge clearance, contact and collision factors, the hinge is in different states under different excitations, resulting in different hinge stiffnesses. The change in the hinge stiffness leads to a change in the overall stiffness of the extension arm. This causes the natural frequency and dynamic response of the coilable mast to vary with the external excitations [31, 32]. Therefore, accurately predicting the model dynamic response while considering hinge nonlinearities is difficult.

2.3 Models of other components

In addition to rotating hinges, a coilable mast also contains other components: longerons, battens and diagonal cables. Longerons and battens can be modelled by beam units in the FEM. However, because they are more flexible than traditional truss structures are, longerons and battens are prone to large geometric deformations under external loads, resulting in geometrical nonlinearity. This problem can be solved by turning on the geometric large deformation switch in commonly used finite element software. Diagonal cables typically have a large tensile stiffness. However, unlike traditional truss structures, diagonal cables cannot withstand compressive loads. This characteristic of diagonal cables can be considered a material nonlinear problem. The diagonal cable material has a nonlinear constitutive relationship: the compressive stress is always 0, and the tensile stress varies linearly with the tensile strain.

Moreover, the modelling of diagonal cables also needs to consider preloads. The initial stress method is a method commonly used to apply preloads, which is realised by adding an initial stress field to diagonal cables. When the initial values of the preloads L_{ini} (the tensions of the diagonal cables during assembly) are known, their initial stress satisfies $\sigma_{ini} = L_{ini}/S_{diag}$, where S_{diag} is the cross-sectional area of the diagonal cable. Therefore, when a coilable mast model is established, an initial stress field should be given first, and then a static balance analysis should be carried out to obtain the rebalanced model. As shown in Fig. 5, Point 1 represents the stress of the diagonal cables under the initial preload, which is not equal to the actual stress of the diagonal cables after assembly of the coilable mast. Point 2 represents the stress of the diagonal cables after rebalancing analysis. The model after rebalancing analysis is the real model that considers the effect of diagonal cable preloads.

3.0 Identification of the hinge equivalent rotational stiffness

In the TMURS hinge model proposed in Section 2.2, the hinge equivalent rotational stiffness K_{hinge} is undetermined. In this section, the identification method for K_{hinge} is proposed.

3.1 Identification method

The hinge equivalent rotational stiffness K_{hinge} is related to the size of the hinge, the preloads of the diagonal cables and the configuration of the coilable mast, which differs for different coilable masts and

2 Segments of a coilable mast
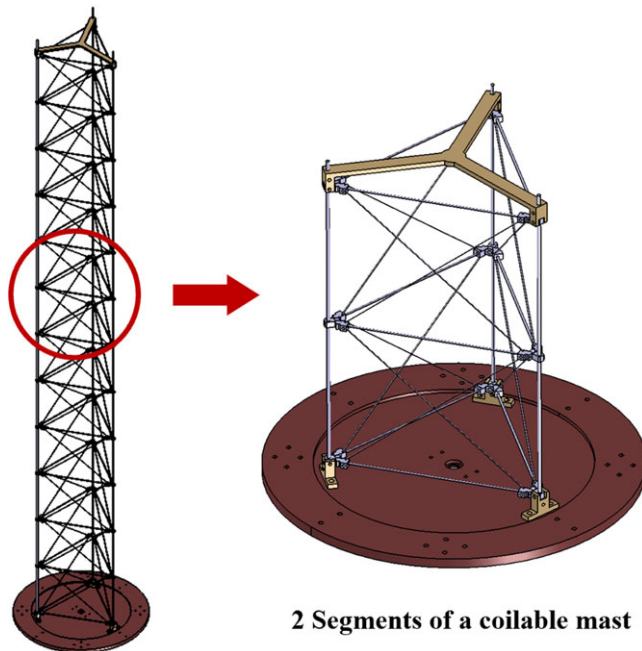
Figure 6. *2-segment scaled object of a coilable mast.*

is difficult to determine directly. Natural frequencies are inherent properties of structures, so K_{hinge} can be identified by targeting the experimental natural frequencies of the coilable mast.

Hammer test method (HTM) is a fast and convenient method for experimental modal analysis of structures and is widely used in engineering applications. Nevertheless, measuring the natural frequencies and modal shapes of a full-length coilable mast via the HTM is ineffective because they are usually too long to measure. Since coilable masts are typical array structures with 'segments' as the unit, single or multiple segments can reflect all their structural characteristics. Therefore, a single segment or multiple segments of the coilable mast can be selected as a scaled object instead of the full-length mast for hinge-equivalent rotational stiffness identification. In this study, two segments are selected to construct the scaled object instead of a single segment because the 2-segment scaled object can reflect the interactions between segments, as shown in Fig. 6. Except for the number of segments, the scaled object is completely consistent with the full-length object, including the configuration, diagonal cable preloads and boundary conditions.

In this way, the hinge equivalent rotational stiffness K_{hinge} is identified through the 2-segment scaled object first and then substituted into the full-length model of the coilable mast to verify its correctness. Specifically, the identification process can be divided into three phases, as shown in Fig. 7.

Phase 1 establishes the relationship between the rotational stiffness K in the dynamic model and the natural frequencies of the 2-segment coilable mast. Since it is difficult to establish an explicit relationship between K and the natural frequencies, the natural frequencies of the model with different values of K are analysed through finite element software, and the curve of the relationship between K and the natural frequencies is fit.

Phase 2 determines the hinge equivalent rotational stiffness K_{hinge} by comparing the analysis and test results of the natural frequencies of the scaled object. In this study, only the first– and second-order natural frequencies are selected as the target response to identify K_{hinge}. The first two modes are first-order torsion and bending modes, and their effective mass fractions are much greater than those of other higher-order modes. Therefore, coilable masts typically undergo first-order torsion and bending vibrations in the real world. Therefore, the model developed by using the first two orders of natural
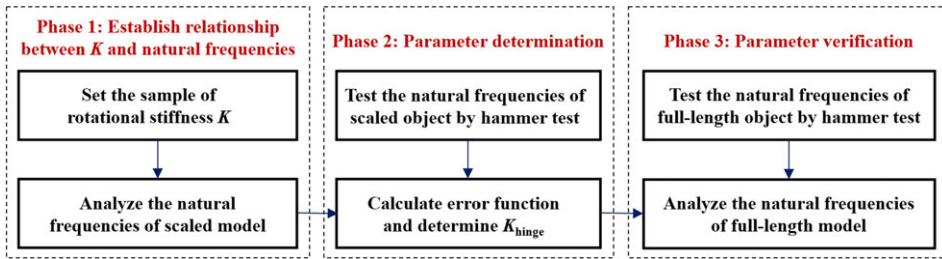
Figure 7. *Flow chart for the identification of the hinge equivalent rotational stiffness.*

Algorithm 1 Pseudocode for the process of identifying the hinge equivalent rotational stiffness K_{hinge}

Step 1.	Give the range of K_{hinge}, and construct the sample space KK: $\{K_1, K_2, \ldots, K_n\}$, where n is the number of samples.
Step 2.	**for** r in range $[1, n]$:
	Establish the scaled model of the coilable mast using K_r;
	Conduct the frequency response analysis to obtain the first- and the second-order natural frequencies $f_1(K_r)$ and $f_2(K_r)$.
	end for
Step 3.	Fit the variation curves of the first- and second-order natural frequencies: $f_1(K)$ and $f_2(K)$.
Step 4.	Calculate the error function $e(K) = \alpha\,|f_1(K) - f_{t1}| + \beta\,|f_2(K) - f_{t2}|$, where $\alpha + \beta = 1$. f_{t1} and f_{t2} are test results of the first- and second-order natural frequencies of the scaled object.
Step 5.	Find the point where $e(K)$ is extremely small; the corresponding K is the hinge equivalent rotational stiffness K_{hinge}.
Step 6.	Establish the full-length coilable mast with K_{hinge}, and compare the analysis and test results of the first- and second-order frequencies to verify the correctness of the identification method.

---

frequencies can reflect the main dynamic behaviour of the coilable mast. If the natural frequencies of the first two modes agree well with the test results, the accuracy of the model is acceptable. The following error function is defined to measure the error between the analysis results and the test results:

$$e = \alpha\,|f_1 - f_{t1}| + \beta\,|f_2 - f_{t2}| \tag{1}$$

where f_1 and f_{t1} are the analysis and test results of the first-order frequency, respectively, and where f_2 and f_{t2} are the analysis and test results of the second-order frequency, respectively. α and β represent the proportions of the first- and second-order frequency errors in the error function, $\alpha + \beta = 1$. When the error function is the minimum, the corresponding rotational stiffness K is the hinge equivalent rotational stiffness K_{hinge}.

Phase 3 involves verifying the correctness of K_{hinge}. The K_{hinge} obtained in Phase 2 to Phase 3 are used, and the full-length coilable mast model is established. Then, the first- and second-order natural frequencies are analysed and compared with the full-length test results to verify the correctness of K_{hinge}.

In summary, the process of identifying the hinge equivalent rotational stiffness K_{hinge} can be illustrated as the pseudocode in the following Algorithm 1.

3.2 Frequency response analysis based on the virtual hammer test

In the process of identifying K_{hinge} in Section 3.1, frequency response analysis is essential for obtaining the first two orders of the natural frequencies of the scaled model or the full-length model of the coilable mast. A virtual hammer test method (VHTM) is proposed in this subsection for frequency response
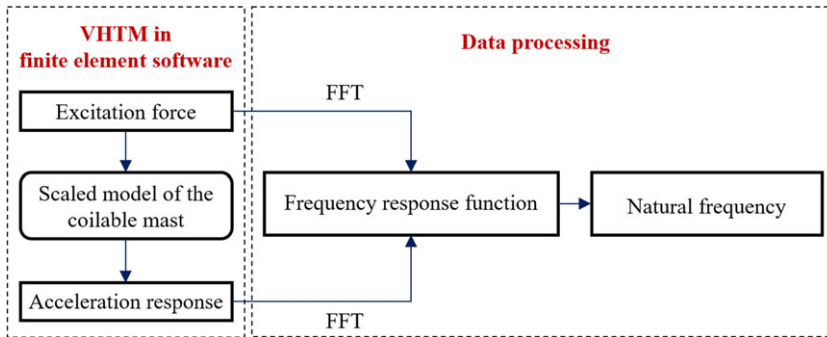
Figure 8. *Flow chart of the frequency response analysis based on the VHTM.*

analysis in the identification process. The VHTM is a method used to measure the frequency response of a structural model by simulating the HTM on a computer. In the VHTM, the hammer signal is simulated according to the hammer test for a real situation, and the response signal is calculated by the finite element software. The reason for using the VHTM instead of the modal analysis method for frequency response analysis is twofold. On the one hand, the use of the VHTM is intended to be consistent with the measurement principle of the HTM. On the other hand, the VHTM is more accurate than the modal analysis method is in determining the frequency response of nonlinear structures such as coilable masts because modal analysis cannot address the stiffness weakening effects of nonlinear components.

The flow chart of the frequency response analysis based on the VHTM is shown in Fig. 8. The analysis steps are as follows:

Step 1: The VHTM is performed via explicit dynamic analysis in finite element software, and the time-domain acceleration response is obtained at the response points. Unlike the multiexcitation input and single-response output (MISO) approach in the HTM, the VHTM adopts the single excitation input and multiresponse output (SIMO) approach. These two approaches are equivalent in frequency response analysis, but SIMO has higher computational efficiency because the response of all points can be obtained by one structural analysis.

Step 2: The frequency response function is solved by using the excitation and response signals obtained from the finite element software. Applying the fast Fourier transform (FFT) technique, the frequency response function is defined as the amplitude ratio of the acceleration response $A_i(\omega)$ to the excitation signal $P_j(\omega)$:

$$R_{ij}(\omega) = A_i(\omega) / P_j(\omega) \tag{2}$$

where ω is the excitation frequency, i and j represent the numbers of response and excitation points, respectively, and $A_i(\omega)$ and $P_j(\omega)$ are the Fourier transforms of $a_i(t)$ and $p_j(t)$, respectively. $a_i(t)$ and $p_j(t)$ are the time domain signals of the response and excitation, respectively. By averaging all the frequency response functions, the overall frequency response function of the structure can be obtained. For the SIMO method, the frequency response function of the structure can be simplified as follows:

$$R_j(\omega) = \frac{1}{n} \sum_{i=1}^{n} R_{ij}(\omega) \tag{3}$$

where j is determined and where n is the total number of response points.

Step 3: The natural frequencies are determined via a graphical method [13]. The graphical method uses the characteristics of frequency response function curves to identify natural frequencies directly. When the frequency response function curve is obtained, the frequencies corresponding to its peaks are determined as the natural frequencies of the structure. The corresponding model shapes refer to the modal analysis results.

Table 1. *Technical parameters of the coilable mast*

Parameter	Value
Coiling radius, R (mm)	100
Pitch length, t (mm)	125
Longeron diameter, d_l (mm)	3
Batten diameter, d_b (mm)	1.8
Segment number, n	12
Diagonal cable cross-section area, S_{diag} (mm^2)	0.79
Diagonal cables initial preload, L_{ini} (N)	40
Hinge mass, m_A/m_B (g)	m_A: 2/m_B: 1.1
Longeron and batten material	Titanium−nickel alloy
Longeron and batten elasticity modulus, E (GPa)	83
Longeron and batten Poisson's ratio, μ	0.31
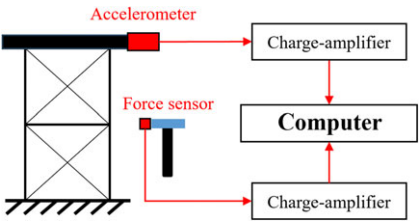


Figure 9. *Schematic diagram of the hammer test.*

4.0 Modelling an example of a coilable mast

In this section, a coilable mast with practical engineering applications is modelled and analysed to verify the proposed modelling method in this paper. ABAQUS FEA is used for the modelling and frequency response analysis of the coilable mast in this study because it is a commonly used finite element software with advantages in solving nonlinear problems and easy secondary development. The use of other finite element software does not affect the implementation and validation of the proposed method in this paper. The specific technical parameters of the coilable mast are shown in Table 1.

4.1 Hammer test conducted on the 2-segment coilable mast

A hammer test was carried out on the 2-segment coilable mast first. Except for the number of segments, the technical parameters of the 2-segment coilable mast in the hammer test were consistent with those of the full-length mast, as shown in Table 1. The schematic diagram and facilities of the hammer test are shown in Figs 9 and 10, respectively. The equipment used in the hammer test includes a force hammer, an accelerometer, two charge amplifiers and a computer. The force sensor was installed at the head of the force hammer to measure the excitation signal. The accelerometer was mounted on the top plate of the mast to measure the response signal under hammer excitation. The excitation signal and the response signal were input into the computer through two charge amplifiers to calculate the frequency response curves of the 2-segment coilable mast.

In the hammer test, each hinge except the bottom three hinges was treated as a node, and each node was divided into two excitation points, radial and tangential. The MISO method was used in the test because it is difficult to measure the acceleration response of all nodes under one excitation. To avoid the specificity of a single hammering excitation, three hammering excitations were performed at each excitation point, and the average of three responses was taken as the response of that point.
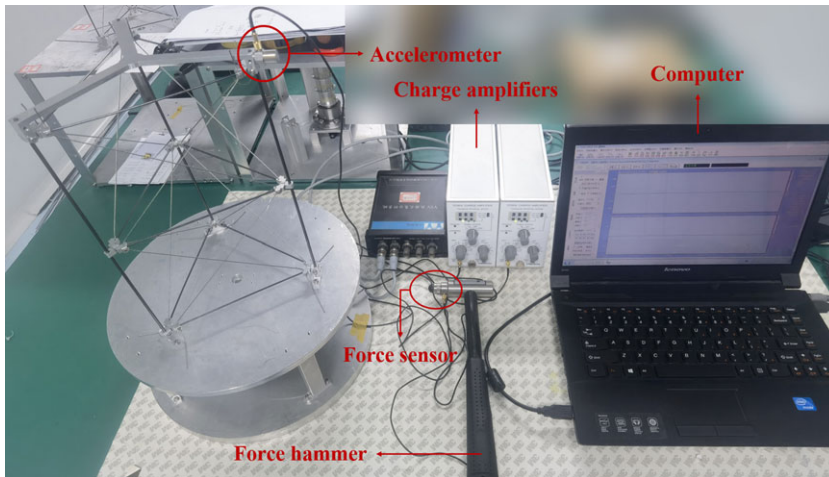
***Figure 10.*** *Facilities of the hammer test (2-segment).*
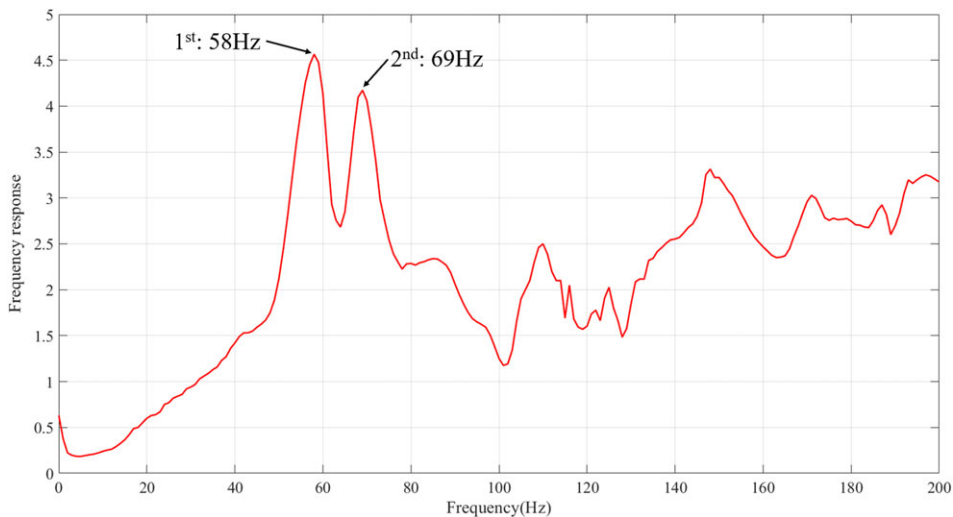
Figure 11. *Frequency response of the 2-segment coilable mast (Test).*

The frequency response curve of the 2-segment coilable mast was obtained, as shown in Fig. 11. As shown in the figure, the first two frequency peaks of the 2-segment coilable mast are obvious, and the corresponding frequencies are 58 Hz and 69 Hz. These two natural frequencies are used as target responses for the identification of the hinge equivalent rotational stiffness K_{hinge}.

4.2 Modelling and parameter identification

According to the modelling methods in Section 2.0, the 2-segment scaled model of the coilable mast was established, as shown in Fig. 12. Figures (a) and (b) show the stress states before and after rebalancing analysis of the coilable mast, respectively. After the rebalancing analysis, the tensions of the diagonal cables change from 40 N to approximately 27.5 N, and there is good consistency in the tensions of the diagonal cables in different segments. The subsequent frequency response analyses based on the VHTM were performed on the rebalanced model.

Then, the range of values for the hinge equivalent rotational stiffness K_{hinge} was given, and the sample space KK: $\{K_1, K_2. . ., K_n\}$ was constructed. In this study, the range of K_{hinge} was $100-5000$ N·mm/rad,

(a) Before rebalancing analysis of the diagonal cables   **(b)** After rebalancing analysis of the diagonal cables
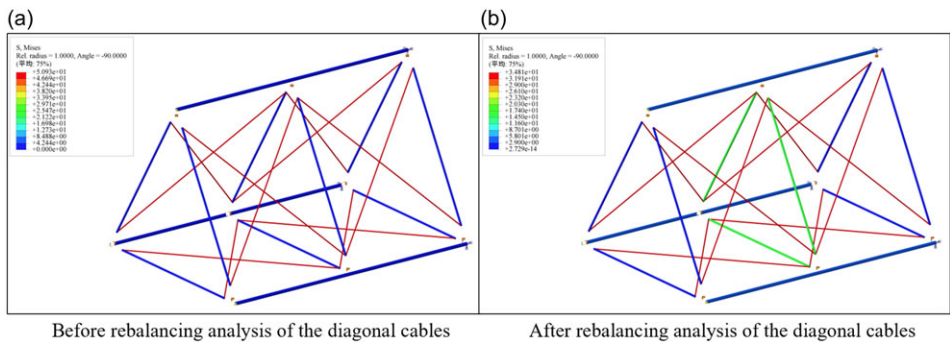
***Figure 12.*** *Dynamic model of the coilable mast (2-segment).*
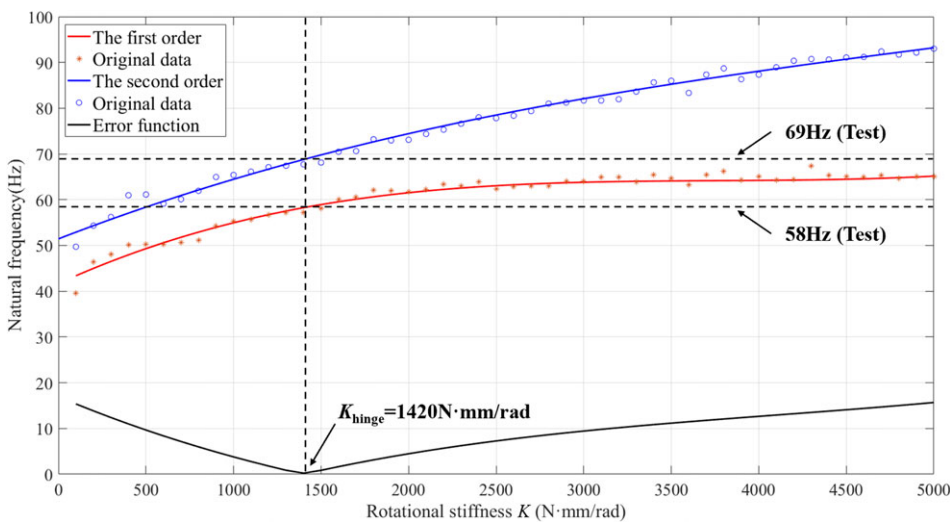
Figure 13. *Curve of the variation in natural frequency with K.*

which is a large range that can ensure that the actual value falls within it. For sample space construction, a linear space containing 50 sample points at intervals of 100 was constructed, which can evenly appraise the effect of hinge rotational stiffness on the response. Moreover, the dimensions of 50 sample points can balance the solving efficiency and the fitting accuracy of the response curve.

A self-developed platform based on the cosimulation technique of MATLAB, Python and ABAQUS FEA was used to automatically model and analyse the frequency response of the coilable mast with different hinge rotational stiffnesses K. Then, the first- and second-order natural frequencies corresponding to different K values were found. Afterwards, the analysis results were fitted using the least squares method to obtain the variation curves of the natural frequencies with respect to the hinge rotational stiffness, as shown in Fig. 13. As shown in the figure, the first-order and second-order frequencies both increase with increasing hinge rotational stiffness K. The difference is that the first-order frequency tends to stabilise gradually with increasing K value, whereas the second-order frequency shows a continuous increase. According to Equation (1), taking both α and β as 0.5 and f_{t1} and f_{t2} as 58 Hz and 69 Hz, the error function can be calculated, and its curve is shown in Fig. 13.

As shown in Fig. 13, the error curve has a minimum point within the given range. The corresponding K of this point is approximated to 1420 N·mm/rad, which is the identified hinge equivalent rotational stiffness K_{hinge}. The 2-segment coilable mast was remodelled and analysed using K_{hinge}, and the results were compared with the test results to preliminarily verify the correctness of the parameter identification
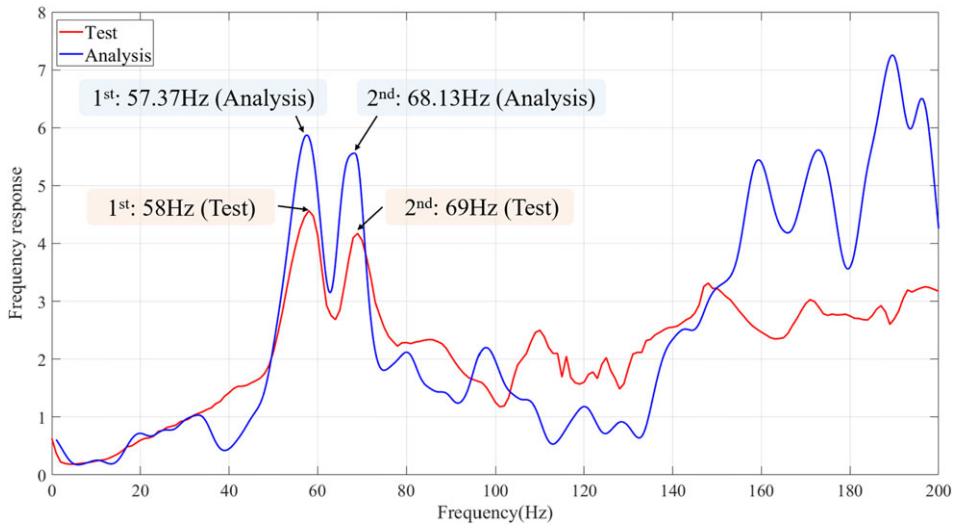
Figure 14. *Comparison of the frequency response curves (2-segment, K = 1,420 N·mm/rad).*

process. A comparison of the frequency response curves obtained from the analysis and test is shown in Fig. 14. As shown in the figure, the analysis results of the first- and second-order natural frequencies are very close to the test results. The relative errors are 1.09% and 1.26%. The analysis of the sources of error are detailed in the next subsection.

In this paper, the damping of the system is ignored in the proposed dynamic model of the coilable mast. There are two main reasons for this: (1) The damping of the structure system is very complicated and difficult to determine directly in the dynamic model; and (2) most deployable structures, such as the coilable mast [32], have very little damping, and ignoring the damping of the structure system does not have much of an effect on the model accuracy. If the damping is considered, then the following relationship is approximately satisfied between the natural frequency and the natural frequency when the damping is ignored: $\omega_d = \omega_n\sqrt{1-\zeta^2}$, where ω_d is the natural frequency when damping is considered, ω_n is the natural frequency when damping is ignored, and ζ is the structural damping ratio. For a structure with low damping, such as a coilable mast, the structural damping ratio satisfies $0 < \zeta < 1$; then, $\omega_d < \omega_n$. At this time, the first- and second-order frequency variation curves in Fig. 13 are lower than the existing curves. Since the experimentally obtained target frequencies used for parameter identification are unchanged, the identified hinge equivalent rotational stiffness K_{hinge} increases. In terms of the change in the frequency response curve in Fig. 14, the amplitude of the analysis curve decreases, but the change in the natural frequency cannot be directly determined. The change in the natural frequency is affected by the joint influence of damping and K_{hinge}, and the natural frequency decreases when the effect of damping is greater and increases when the effect of the change in K_{hinge} is greater.

4.3 Parameter verification

The identification result of the hinge equivalent rotational stiffness ($K_{hinge} = 1,420$ N·mm/rad) was preliminarily verified by a 2-segment coilable mast. In this subsection, the correctness of the identification results is verified by the full-length coilable mast.

The model of the full-length coilable mast is shown in Fig. 15. Figures (a) and (b) reflect the stress states of the coilable mast before and after the rebalancing analysis, respectively. The tensions of the diagonal cables change from 40 N to approximately 24.5 N, the magnitudes of which are close to those of the scaled model and have good consistency in different segments.
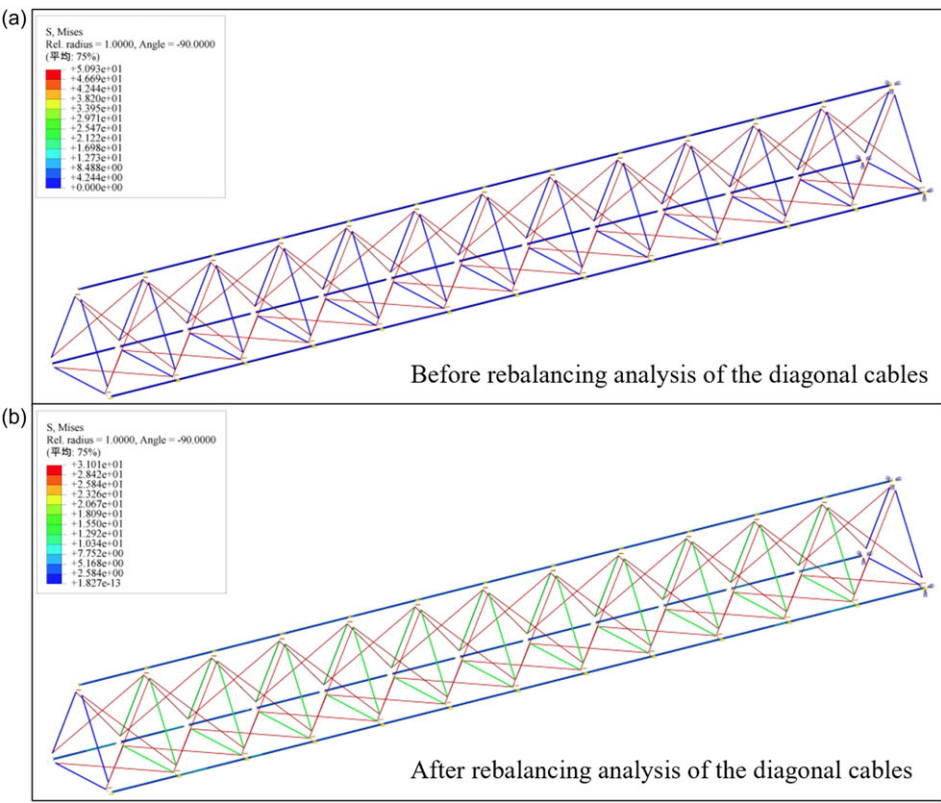
Figure 15. *Dynamic model of the coilable mast (full length).*
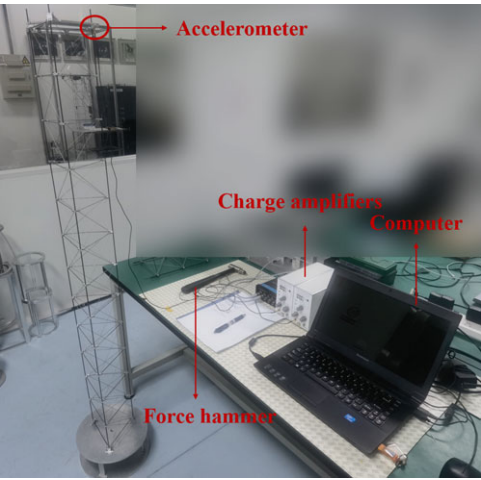
Figure 16. *Facilities of the hammer test (full length).*

First, the first two natural frequencies of the full-length coilable mast were tested. The facilities for the hammer test are shown in Fig. 16. The boundary conditions of the full-length coilable mast and measuring equipment in the hammer test are the same as those in the 2-segment coilable mast test. The test results of the first- and second-order natural frequencies of the full-length coilable mast are 13 Hz and 18 Hz, respectively.
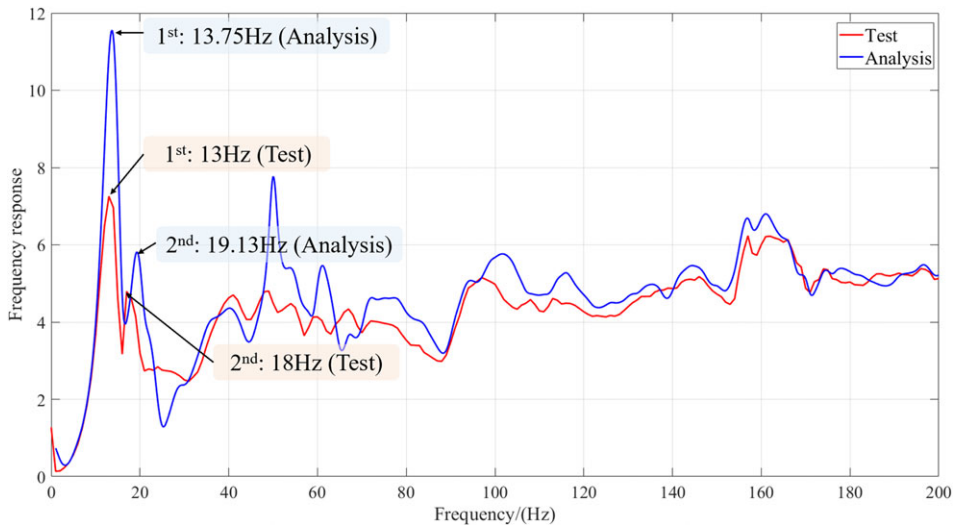
Figure 17. *Comparison of frequency response curves (full length, K = 1,420 N·mm/rad).*

Then, the frequency response analysis based on the VHTM was performed for the coilable mast after rebalancing analysis. The analysis results were compared with the test results, as shown in Fig. 17. The analysis results of the first- and second-order natural frequencies of the full-length coilable mast are 13.75 Hz and 19.13 Hz, respectively. The relative errors with respect to the test results are 5.77% and 6.28%, respectively. Although the relative error is larger than that of the 2-segment model, it is still within a small range, and the frequency response curves of the analysis and test results are close, which verifies the correctness of the identified hinge equivalent rotational stiffness K_{hinge} and the effectiveness of the modelling and identification methods proposed in this paper.

The sources of error are systematically analysed below on the basis of the comparison results shown in Figs. 14 and 17. As shown in the figures, the errors are reflected in two main aspects: (1) the amplitude error of the frequency response curves, and (2) the location error of the natural frequencies. The amplitude error of the frequency response curves is due mainly to ignoring the system damping of the coilable mast model. The sources of the error in the natural frequencies are relatively complex, and we consider that they come from two aspects: (1) parameter identification error and (2) model error. The parameter identification error is related to the number of sample points and the curve fitting accuracy, as shown in Fig. 13. Theoretically, increasing the number of sample points and choosing a more accurate fitting method can improve the parameter identification accuracy, but this approach significantly increases the computational cost. The model error arises from ignoring the model damping as well as the potential nonlinear properties of the hinge. A comparison of the results shown in Figs 14 and 17 reveals that the relative error of the full-length model is larger than that of the 2-segment scaled model. On the one hand, the hinge equivalent rotational stiffness is identified on the basis of the 2-segment scale model, which is slightly different from the hinge stiffness in the full-length model, making the identified stiffness have a larger error in the full-length model. On the other hand, because the damping of the full-length model is greater than that of the 2-segment scaled model and the number of hinges is greater, the model error has a greater effect on the error of the full-length model.

5.0 Discussion and comparison

5.1 Discussion of the effect of changes in the diagonal cable preload

In this subsection, the effect of changes in the diagonal cable preload on the hinge equivalent rotational stiffness is further discussed. The reason for this problem is that changes in diagonal cable preload often

Table 2. *Test results of natural frequencies with different diagonal cable initial preloads*

Diagonal Cable Initial Preload	35 N	40 N	45 N
First-order frequency	55 Hz (Torsion)	58 Hz (Torsion)	60 Hz (Torsion)
Second-order frequency	67 Hz (Bending)	69 Hz (Bending)	71 Hz (Bending)
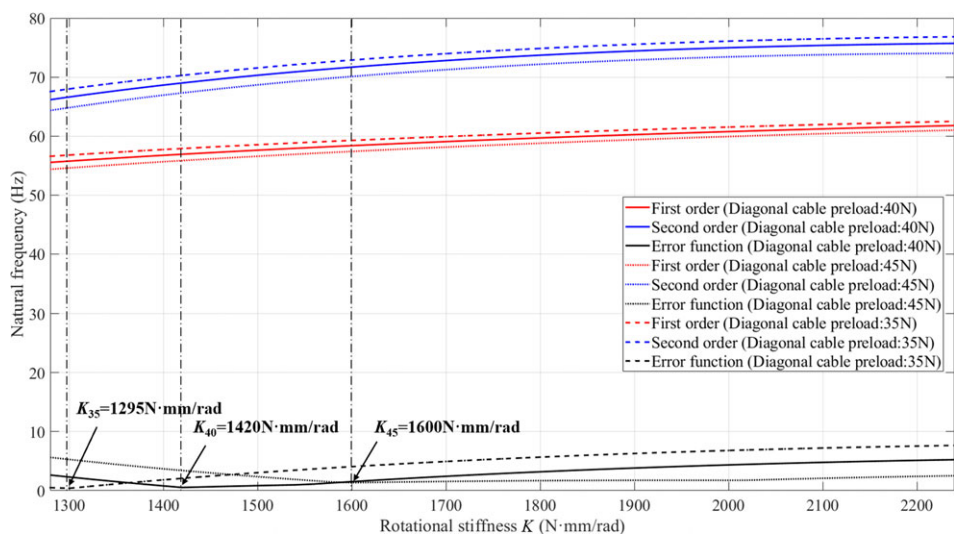
Figure 18. *Comparison of the identified hinge stiffness with different diagonal cable preloads.*

occur in practical engineering. For example, designers can fine-tune the stiffness of the coilable mast by adjusting the diagonal cable preload. To study the effect of the change in diagonal cable preload, three new scaled samples with initial preloads of 35N, 40N and 45N are reassembled for the identification of the hinge equivalent rotational stiffness. According to the process of identifying the hinge equivalent rotational stiffness presented in this paper, hammer tests are conducted first on three scaled samples to measure the first two orders of natural frequencies. The test results are shown in Table 2. With increasing diagonal cable preload, the first two orders of the natural frequencies of the scaled samples increase slightly, which indicates that increasing the diagonal cable preload can improve the overall stiffness of the coilable mast. After that, the VHTM is used to obtain curves of the change in the first two orders of natural frequencies with the rotational stiffness of the hinge for the scaled samples with different diagonal cable preloads, and the respective error functions are calculated according to the test results, as shown in Fig. 18.

Figure 18 shows that at the same rotational stiffness of the hinge, the frequency analytical results decrease with increasing diagonal cable preload. This is mainly because the longerons and battens undergo small deformations with increasing diagonal cable preload, which decreases the overall stiffness of the mast, resulting in a small decrease in the analysed frequencies. However, after combining the test results shown in Table 2 and performing parameter identification, the hinge equivalent rotational stiffness clearly tends to increase with increasing diagonal cable preload, which indicates that when the preload of the diagonal cable increases, the hinges of the coilable mast become more difficult to rotate. On the basis of the above analysis and test results, when the preload of the diagonal cable increases, the effect of the increased hinge equivalent rotational stiffness is greater than that of the decreased stiffness of the longerons and battens, which makes the overall stiffness of the coilable mast still slightly increase. If the rotational stiffness of the hinge is not considered and the stiffness is not identified by experiments, the frequency analysis results decrease only as the diagonal cable preload increases, which is not consistent with the experimental situation. This reinforces the necessity of the modelling method proposed

Table 3. *Comparison of the results of different models*

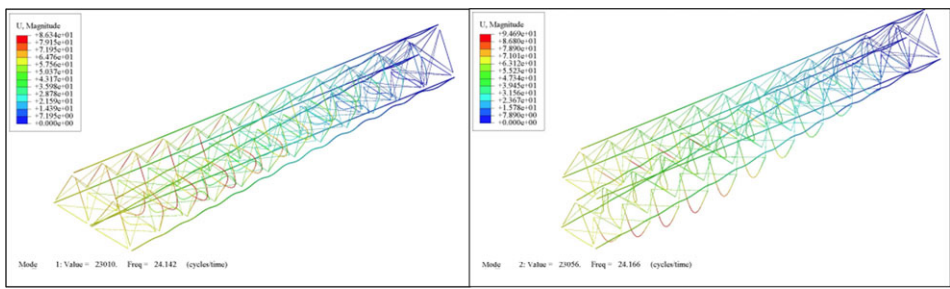| Model	Traditional	This Study	Test
First-order frequency	24.142 (Bending)	13.75 Hz (Torsion)	13 Hz (Torsion)
Second-order frequency	24.166 (Bending)	19.13 Hz (Bending)	18 Hz (Bending)

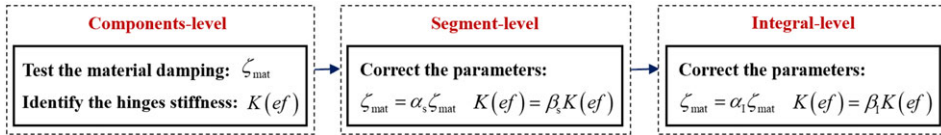***Figure 19.*** *Modal analysis results of the traditional model.*

in this paper to consider the hinge equivalent rotational stiffness and to carry out stiffness identification on the basis of experiments.

5.2 Comparison with the traditional model

To further illustrate the advantages of the dynamic modelling method proposed in this paper, the dynamic model established in this study was discussed and compared with the traditional model. According to previous studies, the traditional model of a coilable mast considers the hinge as a single mass point, which is rigidly connected to the longeron, battens and diagonal cables, regardless of the rotational freedom of the hinge. Moreover, modal analysis is the traditional method for calculating the natural frequencies of a coilable mast. Therefore, the coilable mast introduced in this section was remodelled via the traditional modelling method above and analysed by modal analysis.

The modal analysis results of the traditional model are shown in Fig. 19. Only the first two orders of the natural frequencies are selected for comparison, which are listed in Table 3. As shown in Fig. 19 and Table 3, the first two modes of the traditional model are both bending modes, and the first- and second-order frequencies are 24.142 Hz and 24.166 Hz, respectively. The relative errors between the analysis and test results are 85.71% and 34.26%, respectively. The difference in natural frequencies between the analysis and test results is due to two reasons. On the one hand, the single-mass point model increases the local stiffness of the hinge because it ignores the hinge rotational effect and thus improves the stiffness of the whole structure. On the other hand, the modal analysis method cannot consider the stiffness weakening effect of the nonlinear components inside the coilable mast under external loads, which increases the frequency analysis results compared with the actual situation. The difference in the modal shape is due to the change in the overall stiffness characteristics. The hinge rotational stiffness affects mainly the torsional stiffness of the coilable mast; the smaller the hinge rotational stiffness is, the smaller the torsional stiffness of the coilable mast. This can be verified in the modal analysis; as the hinge torsional stiffness decreases, the first-order mode of the coilable mast changes from the bending mode to the torsion mode. Therefore, when the rotational effect of hinges is considered, the coilable mast is more inclined to undergo torsion rather than bending.

In contrast, the relative errors between the analysis and test results of the dynamic model established via the method proposed in this paper are only 5.77% and 6.28%, respectively. The accuracy of the proposed dynamic model in this study is much higher than that of the traditional model. The traditional model might still be useful in some cases, such as the case of coilable masts with long lengths. The

Components-level	Segment-level	Integral-level
Test the material damping: ζ_{mat} Identify the hinges stiffness: $K(ef)$	Correct the parameters: $\zeta_{\text{mat}} = \alpha_s \zeta_{\text{mat}}$ $K(ef) = \beta_s K(ef)$	Correct the parameters: $\zeta_{\text{mat}} = \alpha_I \zeta_{\text{mat}}$ $K(ef) = \beta_I K(ef)$

Figure 20. *Experimental framework to consider the damping effects and hinge nonlinearities.*

reason for this is that longer coilable masts are prone to bending, and shorter coilable masts are prone to torsion, whereas the traditional model has better accuracy in analysing the frequency of bending modes than torsional modes. Therefore, the traditional model can be applied for frequency response analysis in the case of a coilable mast with a long length, the fundamental frequency is the bending mode, and its analytical accuracy is usually acceptable. However, when the coilable mast is of moderate length and the fundamental frequency is likely to be the first-order torsion mode, the new model proposed in this paper should be used to obtain higher accuracy in frequency response analysis.

6.0 Conclusion

In this paper, a dynamic modelling method based on hinge equivalent rotational stiffness identification is presented. In this method, a dynamic model of an actual coilable mast is established and analysed. The comparison results show that the relative error between the analysis results and test results is acceptable, which proves the correctness and effectiveness of the proposed method. The accuracy of the coilable mast dynamic model established by the method of this paper is greater than that of the traditional model, which can provide a basis for modelling and analysing more complex mechanical systems containing coilable masts and can also provide an accurate dynamic model for the study of vibration control of coilable masts. In addition, the hinge model considering rotational stiffness and its parameter identification method based on scaling experiments proposed in this paper can also provide reference or direct application for other array-type deployable structures containing unlocked hinges, such as 1D and 2D tensegrity deployable structures [33, 34]. Specifically, the designers can also perform hinge rotational stiffness identification by testing the dynamic responses of the array units, and apply the identified rotational stiffness to the overall large deployable structures modelling and dynamic responses prediction.

In future work, we will further improve the modelling accuracy of coilable masts. On the one hand, we will consider the effect of structural damping on model accuracy and explore theoretical or experimental methods to accurately determine the damping parameters of the system. On the other hand, we will consider the potential nonlinear properties of the hinge and establish more accurate nonlinear models to describe the rotational effects of the hinge. A few specific possible treatments as well as an experimental framework are given here to consider the damping effects and the hinge nonlinearities of the model. The damping effects of coilable masts can be considered to originate mainly from material damping ζ_{mat}, which can be tested by equipment such as torsion pendulum meters. The nonlinearities of the hinge mainly originate from the clearance contact and collision. The states of the hinges vary with the external loads, so they will show different stiffness characteristics under different external loads. Therefore, the nonlinearities of the hinge can be characterised by the hinge stiffness that varies with external loads $K(ef)$, which can be identified by the dynamic responses when applying different forms and magnitudes of excitations. Based on the above treatments, the corresponding parameters can be tested or identified by multi-level experiments, and the experimental framework is shown in Fig. 20.

First, an initial determination of the corresponding parameters can be made by component-level tests, including measurements of material damping and stiffness identification of a single hinge. Afterwards, the corresponding parameters are sequentially corrected by correction factors α_s, β_s, α_I and β_I in segment-level and integral-level tests to further refine the values of the parameters in the actual structure. It should be noted that the above experiments should be implemented in a vacuum environment to prevent the influence of air resistance on the accuracy of parameters identification.

References

[1] Fernandez, J.M., Lappas, V.J. and Daton-Lovett, A.J. Completely stripped solar sail concept using bi-stable reeled composite booms, *Acta Astronaut.*, 2011, **69**, (1–2), pp 78–85.

[2] Michael, A.B. A deployable mast for solar sails in the range of 100–1000m, *Adv. Space Res.*, 2011, **48**, pp 1747–1753.

[3] Meguro, A., Shintate, K., Usui, M., et al. In-orbit deployment characteristics of large deployable antenna reflector onboard Engineering Test Satellite VIII, *Acta Astronaut.*, 2009, **65**, (9–10), pp 1306–1316.

[4] Wang, J., Li, D.X. and Jiang, J.P. Finite element modeling and modal analysis of coilable mast, *Appl. Mech. Mater.*, 2012, **226**–**228**, pp 299–302.

[5] Johnson, L., Alexander, L., Fabisinski, L., et al. Multiple NEO rendezvous using solar sail propulsion, in *Proceedings, Global Space Exploration Conference 2012*, International Astronautical Federation (IAF), pp 1–9, 2012.

[6] Eiden, M., Brunner, O. and Stavrinidis, C. Deployment analysis of the Olympus Astromast and comparison with test measurements, *J. Spacecr. Rockets*, 1987, **24**, (1), pp 63–68.

[7] Kitamura, T., Okazaki, K., Natori, M., et al. Development of a "hingeless mast" and its applications, *Acta Astronaut.*, 1988, **17**, (3), pp 341–346.

[8] McEachen, M. Validation of SAILMAST technology and modeling by ground testing of a full-scale flight article, in *48th AIAA Aerospace Sciences Meeting Including the New Horizons Forum and Aerospace Exposition*, American Institute of Aeronautics and Astronautics (AIAA), Report No.: AIAA-2010-1491, pp 1–14, 2010.

[9] Trautt, T. and McEachen, M. Confirmation of non-dimensionalized (scalable) closed-form analytics for modeling slender truss behavior under combined loading, in *48th AIAA Aerospace Sciences Meeting Including the New Horizons Forum and Aerospace Exposition*, American Institute of Aeronautics and Astronautics (AIAA), Report No.: AIAA-2010-1492, pp 1–19, 2010.

[10] Murphy, D.M., Murphey, T.W. and Gierow, P.A. Scalable solar-sail subsystem design concept, *J. Spacecr. Rockets*, 2003, **40**, (4), pp 539–547.

[11] Murphy, D., McEachen, M., Macy, B., et al. Demonstration of a 20-m solar sail system, in *46th AIAA/ASME/ASCE/AHS/ASC Structures, Structural Dynamics and Materials Conference*, American Institute of Aeronautics and Astronautics (AIAA), Report No.: AIAA-2005-2126, pp 1–17, 2005.

[12] Huang, H., Zhao, X., Sun, L., et al. System design and on-orbit test of Student Small Satellite (SSS-1), *Chin. J. Aeronaut.*, 2022, **43**, (10), pp 269–279.

[13] Ishimura, K., Minesugi, K., Kawano, T., et al. On orbit structural performance of Hitomi (ASTRO-H), in *AIAA Scitech 2019 Forum*, American Institute of Aeronautics and Astronautics (AIAA), Report No.: AIAA-2019-0202, pp 1–9, 2019.

[14] Ishimura, K., Ishida, M., Kawano, T., et al. Induced vibration of high-precision extensible optical bench during extension on orbit. *Trans. Jpn. Soc. Aeronaut. Space. Aerosp. Technol. Jpn.*, 2018, **16**, (2), pp 181–187.

[15] Kawano, T., Ishimura, K., Iizuka, R., et al. Validation of on-orbit thermal deformation and finite element model prediction in X-ray astronomical satellite Hitomi, *Trans. Jpn. Soc. Aeronaut. Space Sci. Aerosp. Technol. Jpn.*, 2018, **16**, (3), pp 242–247.

[16] Deininger, W.D., Kalinowski, W., Allen, Z., et al. Imaging X-Ray polarimeter explorer mission spacecraft implementation concept, in *AIAA SPACE and Astronautics Forum and Exposition*, American Institute of Aeronautics and Astronautics (AIAA), Report No.: AIAA-2017-5314, pp 1–10, 2017.

[17] Weisskopf, M.C., Ramsey, B., O'Dell, S.L., et al. The imaging x-ray polarimetry explorer (IXPE). *Results Phys.*, 2016, **6**, pp 1179–1180.

[18] Ma, H., Huang H., Han, J., et al. Study on the criterion to determine the bottom deployment modes of a coilable mast, *Acta Astronaut.*, 2017, **141**, pp 89–97.

[19] Liu, Y., Sun, L., Huang, H., et al. Nonlinear characteristics of torsional stiffness of a coilable mast with triangular section, *Chin. J. Aeronaut.*, 2024, **37**, (10), pp 313–324.

[20] Liu, T., Han, H., Ji, B., et al. Experimental investigation and numerical simulation on nonlinear buckling mode of coil-able mast, *J. Nanjing Univ. Aeronaut. Astronaut.*, 2015, **47**, (6), pp 897–903.

[21] Jin, Y., Liu, T., Lyu, R., et al. Theoretical analysis and experimental investigation on buckling of FASTMast deployable structures, *International Journal of Structural Stability and Dynamics*, 2014, **15**, (5), p 1450075.

[22] Xue, Y. and Liu, Z. Analysis of equilibrium with friction of an elastic rod constrained by a cylindrical surface, *Chin. Q. Mech.*, 2016, **37**, (1), pp 139–148.

[23] Han, J., Wang, X. and Ma, H. Mechanical principle of the deploying mode for coilable mast, *J. Beijing Univ. Aeronaut. Astronaut.*, 2013, **39**, (9), pp 1168–1173.

[24] Han, J., Huang, H. and Ma, H. Vibration model of coilable mast considering slack diagonals, *J. Beijing Univ. Aeronaut. Astronaut.*, 2014, **40**, (7), pp 970–977.

[25] Fan, P., Chen, W., Zhang, Y., et al. FEM analysis on the nonlinear vibration properties of a coilable mast, *J. Vibrat. Shock*, 2018, **37**, (10), pp 80–86.

[26] Zhang, J., Guo, H., Liu, R., et al. Nonlinear dynamic modeling and analysis for space deployable structure with clearance joints, *J Xi'an Jiaotong Univ.*, 2013, **47**, (11), pp 113–119+126.

[27] Li, T., Guo, J. and Cao, Y. Dynamic characteristics analysis of deployable space structures considering joint clearance. *Acta Astronaut.*, 2011, **68**, (7–8), pp 974–983.

[28] Dubowsky, S. and Freudenstein, F. Dynamic analysis of mechanical systems with clearances, part 1: formation of dynamic model, *J. Eng. Ind.*, 1971, **93**, (1), pp 305–309.

[29] Dubowsky, S. and Freudenstein, F. Dynamic analysis of mechanical systems with clearances, part 2: dynamic response, *J. Eng. Ind.*, 1971, **93**, (1), pp 310–316.

[30] Bauchau, O.A. and Rodriguez, J. Modeling of joints with clearance in flexible multibody systems, *Int. J. Solids Struct.*, 2002, **39**, (1), pp 41–63.

[31] Zhang, J. Modeling and analysis of nonlinear dynamics for joint and deployable structure, *Doct. Dissertation Harbin Inst. Technol.*, Harbin Institute of Technology, pp 1–151, 2014.

[32] Zhou, S. and Zhou, X. Development and technical difficulties of deployable space masts, *Chin. Space Sci. Technol.*, 2014, **34**, (6), pp 38–50.

[33] James, V.H., Robert, E.S. and John V. Shape control of tensegrity structures, in *AIAA SPACE 2015 Conference and Exposition*, American Institute of Aeronautics and Astronautics (AIAA), Report No.: AIAA-2015-4502, pp 1–21, 2015.

[34] Tibert, A.G. and Pellegrino, S. Deployable tensegrity reflectors for small satellites, *J. Spacecr. Rockets*, 2002, **39**, (5), pp 701–709.